12-16-2014

Mapping Thunder Sources by Inverting Acoustic and Electromagnetic Observations

J. F. Anderson
New Mexico Institute of Mining and Technology

J. B. Johnson
Boise State University

R. O. Arechiga
New Mexico Institute of Mining and Technology

R. J. Thomas
New Mexico Institute of Mining and Technology

AGU PUBLICATIONS

JGR

Journal of Geophysical Research: Atmospheres

RESEARCH ARTICLE

10.1002/2014JD021624

Key Points:
- Thunder is the weighted sum of acoustic signals from different parts of a flash
- Thunder can be inverted to find source energy of each channel in the flash
- This method can locate current flow in lightning

Correspondence to:
J. F. Anderson,
ajakef@gmail.com

Citation:
Anderson, J. F., J. B. Johnson, R. O. Arechiga, and R. J. Thomas (2014), Mapping thunder sources by inverting acoustic and electromagnetic observations, *J. Geophys. Res. Atmos.*, *119*, 13,287–13,304, doi:10.1002/2014JD021624.

Received 7 FEB 2014
Accepted 13 NOV 2014
Accepted article online 19 NOV 2014
Published online 11 DEC 2014

Mapping thunder sources by inverting acoustic and electromagnetic observations

J. F. Anderson[1], J. B. Johnson[2], R. O. Arechiga[3], and R. J. Thomas[3]

[1]Department of Earth and Environmental Sciences, New Mexico Institute of Mining and Technology, Socorro, New Mexico, USA, [2]Department of Geosciences, Boise State University, Boise, Idaho, USA, [3]Department of Electrical Engineering, New Mexico Institute of Mining and Technology, Socorro, New Mexico, USA

Abstract We present a new method of locating current flow in lightning strikes by inversion of thunder recordings constrained by Lightning Mapping Array observations. First, radio frequency (RF) pulses are connected to reconstruct conductive channels created by leaders. Then, acoustic signals that would be produced by current flow through each channel are forward modeled. The recorded thunder is considered to consist of a weighted superposition of these acoustic signals. We calculate the posterior distribution of acoustic source energy for each channel with a Markov Chain Monte Carlo inversion that fits power envelopes of modeled and recorded thunder; these results show which parts of the flash carry current and produce thunder. We examine the effects of RF pulse location imprecision and atmospheric winds on quality of results and apply this method to several lightning flashes over the Magdalena Mountains in New Mexico, USA. This method will enable more detailed study of lightning phenomena by allowing researchers to map current flow in addition to leader propagation.

1. Introduction

Lightning strikes begin with the propagation of ionized channels called stepped leaders in areas with strong electric fields. These leaders grow through series of ionization events (referred to as steps) that lengthen the ionized channel in random directions beyond the original extent. These steps are separated by several microseconds in time and tens of meters in space. In this manner, leaders form tortuous, dendritic structures that are electrically conductive [*Uman*, 1987]. If one of these conductive channels reaches the ground, the flash is referred to as cloud to ground (CG); otherwise, it is called intracloud (IC). Any channel may carry current, but few typically do; only 35% of one study's CG flashes were observed to contain more than a single current-carrying channel [*Valine and Krider*, 2002].

Two distinct processes produce thunder, each affecting a different frequency band. Audible and near-infrasonic thunder is produced mainly by rapid heating of conductive lightning channels in response to current flow [*Few*, 1969]. During a typical lightning strike, a current pulse on the order of 3×10^4 A travels along conductive channels. This current rapidly heats the surrounding air (3×10^4 K in 5×10^{-6} s) and raises the surrounding pressure to around 10^6 Pa. The intense overpressure forms a shock wave that propagates supersonically (up to 3300 m s^{-1}) [*Rakov and Uman*, 2003]. While additional shock waves may be generated by subsequent strokes, the time separating these strokes (on the order of 4×10^{-2} s) is long enough that shock waves from different strokes are spatially separated and do not interact with one another [*Few*, 1974]. These shock waves quickly decay to acoustic waves. As a result, each stroke radiates acoustic waves along the length of the current-carrying channel. Recordings of thunder from IC events feature lower amplitudes and lower peak frequencies than recordings of thunder from CG strikes [*Holmes et al.*, 1971; *Johnson*, 2012].

Below frequencies of about 2.5 Hz, thunder is dominated by an electrostatic relaxation of the cloud instead of by rapid thermal expansion [*Balachandran*, 1979]. Before a strike can occur, a substantial charge must accumulate in a cloud. Electrostatic forces cause these charged particles to repel one another. When current flow in lightning depletes these charges, the electrostatic repulsion forces decrease, and charged particles are drawn inward, producing a low-frequency acoustic rarefaction propagating as a planar wave with vertical incidence below the cloud [*Dessler*, 1973]. However, subsequent researchers observed a compression pulse before the rarefaction pulse, sometimes followed by additional compression pulses [*Balachandran*, 1979, 1983; *Bohannon et al.*, 1977]. This study attempts to locate current flow and model

thunder from thermal expansion; therefore, we do not address the charge relaxation mechanism in this paper.

Previous studies have attempted to locate thunder sources by obtaining slowness vectors from array recordings, finding lightning strike time from electromagnetic observations and backpropagating the thunder recordings accordingly [*Few*, 1970; *Few and Teer*, 1974; *Teer and Few*, 1974; *MacGorman et al.*, 1981; *Arechiga et al.*, 2011; *Johnson et al.*, 2011]. The general shapes and locations of thunder sources from the last two studies were confirmed by comparison to maps of radio frequency (RF) pulses from leaders. However, the raypaths (and backpropagated source locations) are sensitive to atmospheric temperature and wind structure, which is typically poorly constrained. Consequently, acoustic data alone cannot unambiguously reveal thunder source locations.

The New Mexico Tech Lightning Mapping Array (LMA) has proven a valuable tool for studying lightning over the past decade. The LMA consists of networked antennas that detect and locate RF pulses produced by ionization events in stepped leaders [*Rison et al.*, 1999]. RF pulses above the network are located with an uncertainty of 6–12 m root mean square (RMS) in the horizontal plane and 20–30 m RMS in the vertical direction [*Thomas et al.*, 2004]. These pulses are vertices in the stepped leader structure and can therefore be used to reconstruct the leaders. Knowledge of the stepped leader structure of the strike is useful in modeling thunder, because audible and near-infrasonic thunder comes from current flow along some subset of these channels. Therefore, LMA pulse locations are used to constrain thunder source locations in this method.

One potential bias associated with the LMA is that RF pulses produced by positive electrical breakdown in a negative charge region are less intense than RF pulses produced by negative breakdown in a positive charge region. As a result, ionization events might not be detected equally in the two charge regions. However, subsequent re-ionization events can have different polarity from the original breakdown so that detectable ionization events occur along all parts of the strike. In practice, this issue was not problematic in our LMA deployment: sufficient RF pulses were located in both regions for this method to accurately and completely delineate the channels.

Acoustic modeling requires knowledge of the propagation medium's structure. Unfortunately, thunderstorm atmospheric structures can be complicated and difficult to measure. Storms require unstable air to form and persist, so the temperature lapse rate in a thunderstorm must exceed the moist adiabatic lapse rate (5–10°C km^{-1}, depending on humidity). Because the intrinsic sound speed in air is proportional to the square root of temperature, sound speed must also decrease with elevation, which causes acoustic waves to be refracted upward. Consequently, thunder is rarely heard more than 25 km from a flash, because refraction prevents the thunder from reaching the ground beyond that point [*Fleagle*, 1949]. On the other hand, low-level atmospheric structures below the storm, such as inversions, could amplify thunder generated at low elevations.

Additionally, thunderstorms often include intense and sheared wind. Wind affects the speed at which sound propagates and can have refractive effects of equal importance to those of the temperature lapse rate [*Fleagle*, 1949]. Refraction from wind and temperature in these heterogeneous, anisotropic structures affects arrival time and amplitude of acoustic waves. Because thunderstorm temperature and wind information is not commonly available above the surface, predicting refractive effects on thunder signals is generally not possible.

Other propagation effects further alter thunder signals. In high-amplitude waves, such as thunder close to the source, the linear acoustic wave equation becomes invalid, and nonlinear propagation effects (mainly advection of momentum and energy by wave crests) cause compressions to propagate faster than the normal speed of sound. Because thunder waves begin with compressions, the front travels faster than the rest of the wave, making the wave lengthen as it propagates. This nonlinear effect can be significant up to 1 km away from thunder sources [*Otterman*, 1959]. Turbulence is another common complication of thunderstorm atmospheres, although its consequences to sound wave propagation are difficult to quantify. Multipathing by topographic scattering can further complicate thunder; however, due to the computational expense of calculating reflected raypaths, and the lower amplitudes of scattered waves compared to direct arrivals, it is not considered here. Another factor (mainly affecting high frequencies) is intrinsic attenuation, which dissipates energy in acoustic waves. Attenuation is roughly equal to an elevation-dependent coefficient times

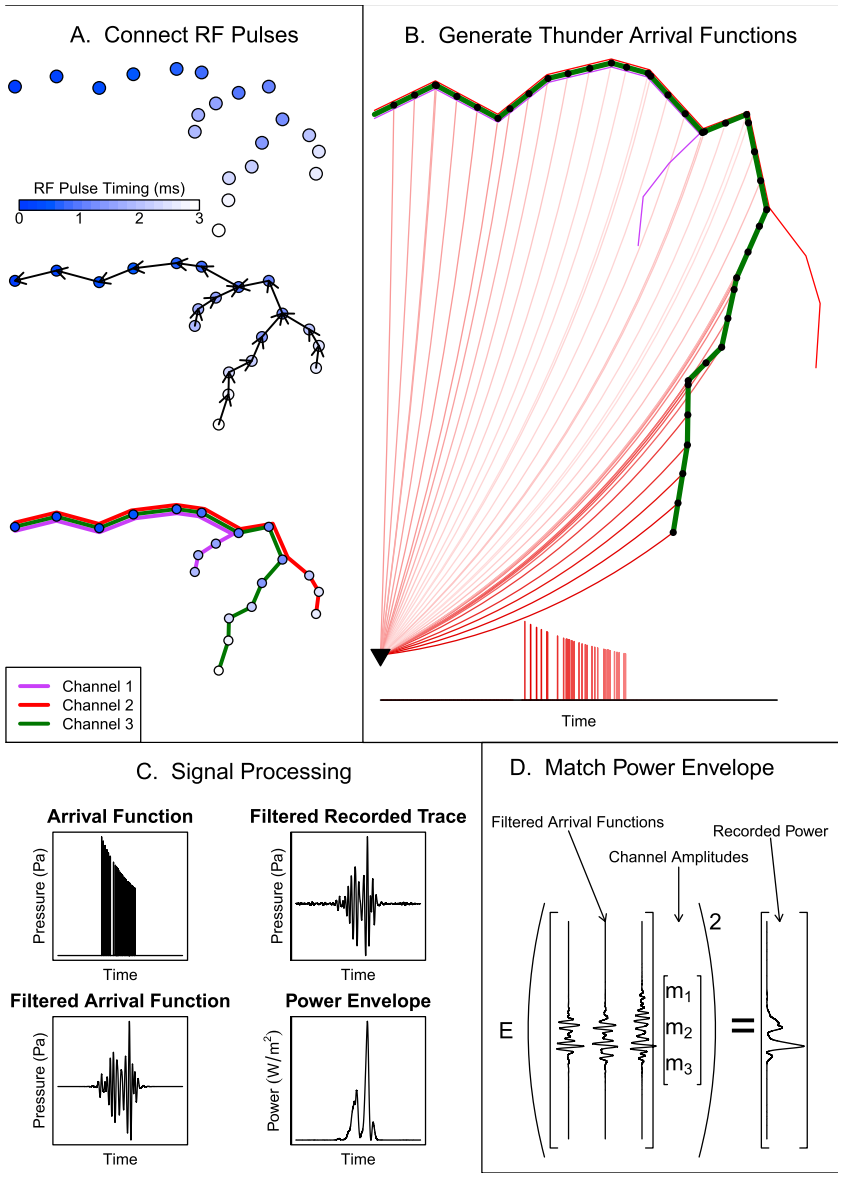

Figure 1. Schematic outline of the inversion method using synthetic data. (a) Each RF pulse is connected to its nearest neighbor that occurs earlier in time. These connections can be traced backward to reconstruct conductive channels. (b) Each channel (here channel 3) is discretized as a set of finely spaced interpolated acoustic sources. Travel times and amplitudes are calculated for waves propagating from each source to the receiver. These arrivals are represented as time-shifted, amplitude-scaled delta functions and are superposed to form an arrival function. (c) Arrival functions are filtered, and the power envelope is calculated for the filtered recorded data. (d) A nonlinear inversion is performed to match the power envelope of a weighted superposition of filtered arrival functions to the power envelope of the recorded data.

frequency squared, and it never exceeds 7.35×10^{-2} dB/km over the low elevations and frequencies studied here (less than 24 Hz and less than 12 km) [*Sutherland and Bass*, 2004; *de Groot-Hedlin*, 2008]. The flashes studied here occur within 12 km of the microphones, so no interesting part of our signals is ever attenuated by more than 2 dB, and the bulk of the signals is attenuated much less than that. Because the effect of attenuation on our signals is weak, it is not considered here.

2. Description of Method

This inversion method locates and quantifies thunder generation in lightning flashes (Figure 1). It requires RF pulse locations (computed by the LMA) and acoustic recordings of thunder. We identify conductive channels

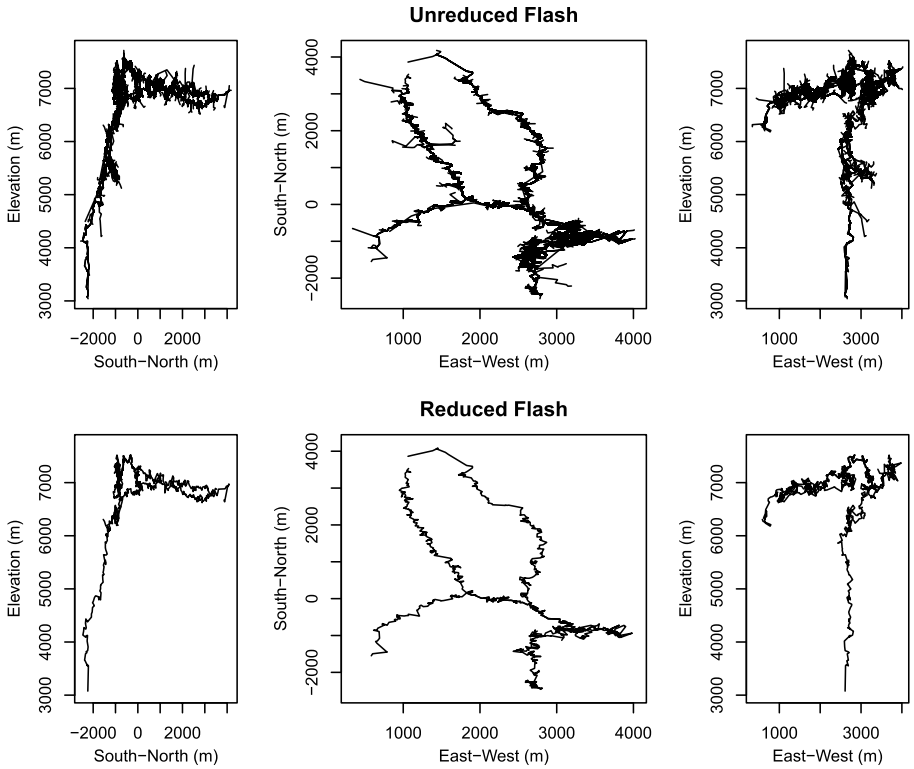

Figure 2. The number of channels in a flash can be reduced by discarding those with short independent length. This reduces the computational expense of forward modeling thunder signals, as well as reducing the number of free parameters in the inverse problem. In this flash, the number of channels to consider was reduced from 431 to 7.

by connecting RF pulses (section 2.1), and, assuming a reasonable atmosphere, forward model the acoustic signal that would be recorded for each conductive channel (section 2.2). Treating the thunder as a weighted superposition of the channels' acoustic signatures, we then invert to find the acoustic amplitude of each channel that optimizes the fit of modeled thunder power envelopes to recorded thunder power envelopes (section 2.3). Because the true structure of the atmosphere around the strike is unknown, we repeat this process many times, over many reasonable atmospheres, until an optimal fit is found.

2.1. Conductive Channel Identification

The LMA provides a catalog of RF pulses occurring during an event but does not show the conductive channels connecting them. In order to reconstruct conductive channels, we use the principle that leaders may branch as they propagate but do not merge. Consequently, each vertex in a leader can connect to any number of later vertices (representing branching) but at most one earlier vertex. For each RF pulse, we find its nearest earlier neighbor and connect them. Additionally, because conductive channels may be reactivated by subsequent stepped or dart leaders, RF sources that occur along a preexisting conductive channel are merged into that channel. In this way, conductive channels may be traced backward from their terminal vertices to their beginnings.

One consequence of this scheme is that conductive channels may overlap in the early sections of the leader. This is desirable, because current flow through either will correctly imply thunder production from their overlapped section. In the case of multiple overlapping channels carrying current, the acoustic source amplitude of their overlapped sections is the linear sum of the source amplitudes of the individual channels. This follows from thunder in the near-infrasound and audible bands being produced by resistive heating during current flow [*Few*, 1969], which must be conserved throughout the channel structure.

The number of conductive channels to consider can be reduced (Figure 2) by eliminating "dead-end" channels whose independent segments (i.e., segments that do not overlap with longer channels) are short. These dead ends are leaders that branched from another channel but failed to propagate far and therefore are

unlikely to carry current. Removing dead ends is advantageous for two reasons: it reduces the number of parameters in the model and reduces the computational expense of modeling thunder signals. This process may decrease the number of channels from hundreds to less than 10, depending on the independent segment length threshold used for dead-end identification. The threshold needed to eliminate dead ends but not the main channels depends on the scale of the strike; for each strike studied here, we picked an optimal threshold that reduced strike complexity while preserving core channels. Additionally, for CG events the entire set of channels formed by downward propagating leaders before the first return stroke must be considered because of the possibility of charge deposition along the entire structure during the first return stroke. Therefore, we include that structure (including dead ends) as a potential acoustic source in addition to the main channels identified by dead-end elimination.

2.2. Acoustic Forward Modeling

Each conductive channel may be regarded as a string of finely spaced (in this work, every 1 m) acoustic point sources; this approximation is valid as long as the spacing is short compared to the wavelengths studied (from about 25 m to 60 m for the 6–12 Hz band studied here). For each point source, we use standard ray tracing equations [*Garces et al.*, 1998; *Anderson*, 2013] to calculate travel time and arrival amplitude of signals from each point source. Time of thunder generation is determined by electromagnetic observations; in this work, we used electrical interference produced by lightning current flow and recorded by our unshielded sensor cables, but RF pulse timing could be used as well. Typically, multiple strokes are detected during a flash. However, the errors associated with propagation through complicated atmospheres make the relatively small intervals between strokes unresolvable. Therefore, only a single source time (the mean time of all strokes) is used in these calculations. We construct an "arrival function" by superposing impulses whose timing and amplitude correspond to those of arrivals associated with each point source.

To convert this arrival function into a true pressure signal, we would need to convolve it with a source time function, which is unconstrained. However, the channel heating and expansion that produces thunder occurs rapidly, and we ultimately band-pass filter these models and recordings to low frequencies, so the source time function can be treated as being approximately impulsive. Band-pass filtering also eliminates the need to consider attenuation, which has little effect on low frequencies at these distances.

Phase coherence between recorded thunder and modeled signals is probably weak for these frequencies because our assumed source time functions and atmospheres are not exact. Because of this, we calculate the power envelope of recorded and modeled signals before comparing them; this makes signal comparison less sensitive to small timing errors in modeled signals. This forward modeling procedure is repeated for each microphone in the network and each conductive channel, giving us a set of signals each microphone would record for each conductive channel.

2.3. Inversion for Channel Source Amplitudes

Thunder can be treated as a weighted superposition of different channels' acoustic signatures. To determine the weight of each channel, we concatenate signals for different microphones (so that all data to be fit are contained in a single vector) and perform a nonlinear inversion using the Metropolis-Hastings Markov Chain Monte Carlo (MCMC) method [*Hastings*, 1970; *Aster et al.*, 2012] to minimize the misfit between modeled and observed power envelopes. This method has important advantages over other nonlinear inverse methods, including its ability to return a posterior distribution of model parameters and its robustness against returning locally (not globally) optimal models. Using the notation $\mathbf{G}$ for a matrix whose columns are forward modeled thunder signals, $\mathbf{m}$ for a vector of acoustic source amplitudes, $\mathbf{r}$ for a recorded thunder time series, and E for the power envelope function, we invert to find $\mathbf{m}$ that minimizes the normalized data misfit

$$\frac{\|E(\mathbf{Gm}) - E(\mathbf{r})\|_2}{\|E(\mathbf{r})\|_2} \tag{1}$$

which is the ratio between the L^2 norm of the difference between observed and modeled power envelopes and the L^2 norm of the observed power envelope.

This MCMC implementation consists of 50,000 iterations in which a random model parameter is perturbed by multiplication by a positive random number drawn from a lognormal distribution centered at 1. Because negative parameter values indicate unrealistic rarefactions instead of compressions radiating from lightning channels, we require that all model parameters be nonnegative. This method of parameter perturbation accomplishes that. In each iteration, misfit between modeled and recorded data is calculated. The proposed

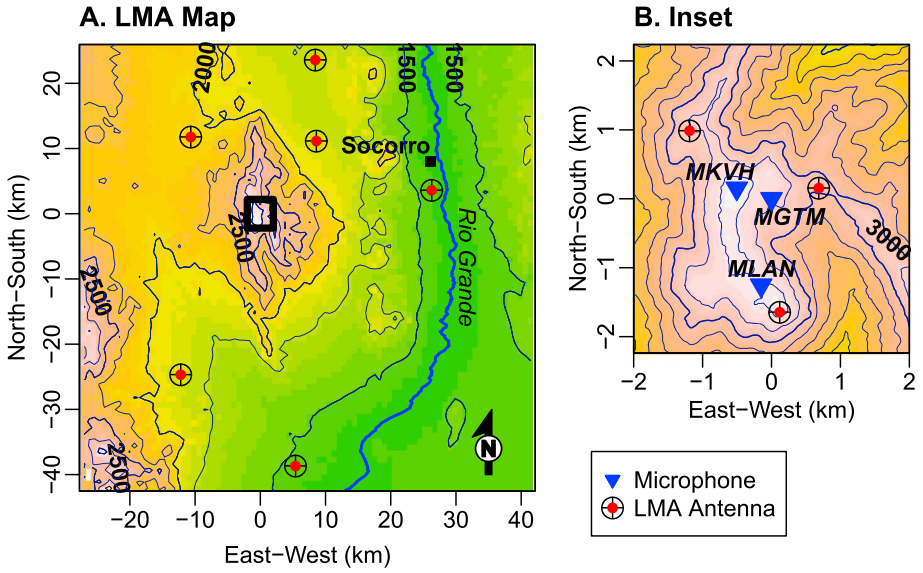

Figure 3. Map of sensor deployment used in this experiment in central New Mexico, USA. (a) The LMA consisted of a "regional" component consisting of six antennas spaced around the Magdalena Mountains at distances of more than 10 km and a "local" component including three antennas deployed close together high in the mountains. (b) The acoustic network included three broadband microphones deployed in the same area as the local part of the LMA (within the black square). The MGTM station is used as the origin of the map.

model parameter is always accepted if it decreases the misfit. Additionally, the proposed model parameter could be accepted if it increases the misfit, with probability of acceptance decreasing with higher differences in misfit. In practice, our acceptance ratios varied between 0.1 and 0.7. We have no prior information about the acoustic energy release of the lightning channels and therefore use an uninformative prior model. After running 50,000 iterations, we consider the first 25,000 to be a "burn-in" period in which the influence of the initial model has not been completely lost and discard them. Then, to reduce correlation between successive iterations, only every tenth iteration is sampled. The models in these remaining iterations reflect the posterior distribution of the model and show the likelihoods of acoustic source amplitude values and the covariance among different conductive channels.

3. Experiment

3.1. Deployment and Data

We analyze data from a 2009 instrument deployment in the Magdalena Mountains in central New Mexico. Twelve broadband (< 0.1 Hz to a Nyquist frequency of 500 Hz) Infra-NMT microphones with flat frequency responses [*Marcillo et al.*, 2012] were deployed in three arrays (MGTM, MKVH, and MLAN) consisting of four microphones each (Figure 3). Microphone arrays were in a triangular configuration with three peripheral and one central microphone connected by cable to a RefTek RT-130 data logger recording 1000 samples per second at 24 bits. Because of the close spacing of the microphones within the arrays, acoustic data from the central microphones only are considered here (although, for determining strike timing, electrical interference recorded on all acoustic channels is considered). Recordings were converted to overpressure units before analysis. Additionally, we used electromagnetic data from nine LMA sensors, with three forming a local component to the array (within 2 km of the acoustic network center) and another six forming a regional component (within 30 km of the acoustic network center). The LMA and microphone arrays both received precise timing information from GPS antennas.

We present results from several flashes during a storm that occurred on 24 July 2009. We examine in particular detail a CG flash that occurred at 19:42:13 UTC. This strike included 2555 RF sources that were connected to form 431 conductive channels. The vast majority of these channels are probably inactive dead ends because of their short independent lengths. In order to simplify the strike and remove these channels from consideration, all channels whose independent length fell below a threshold of 4500 m were ignored;

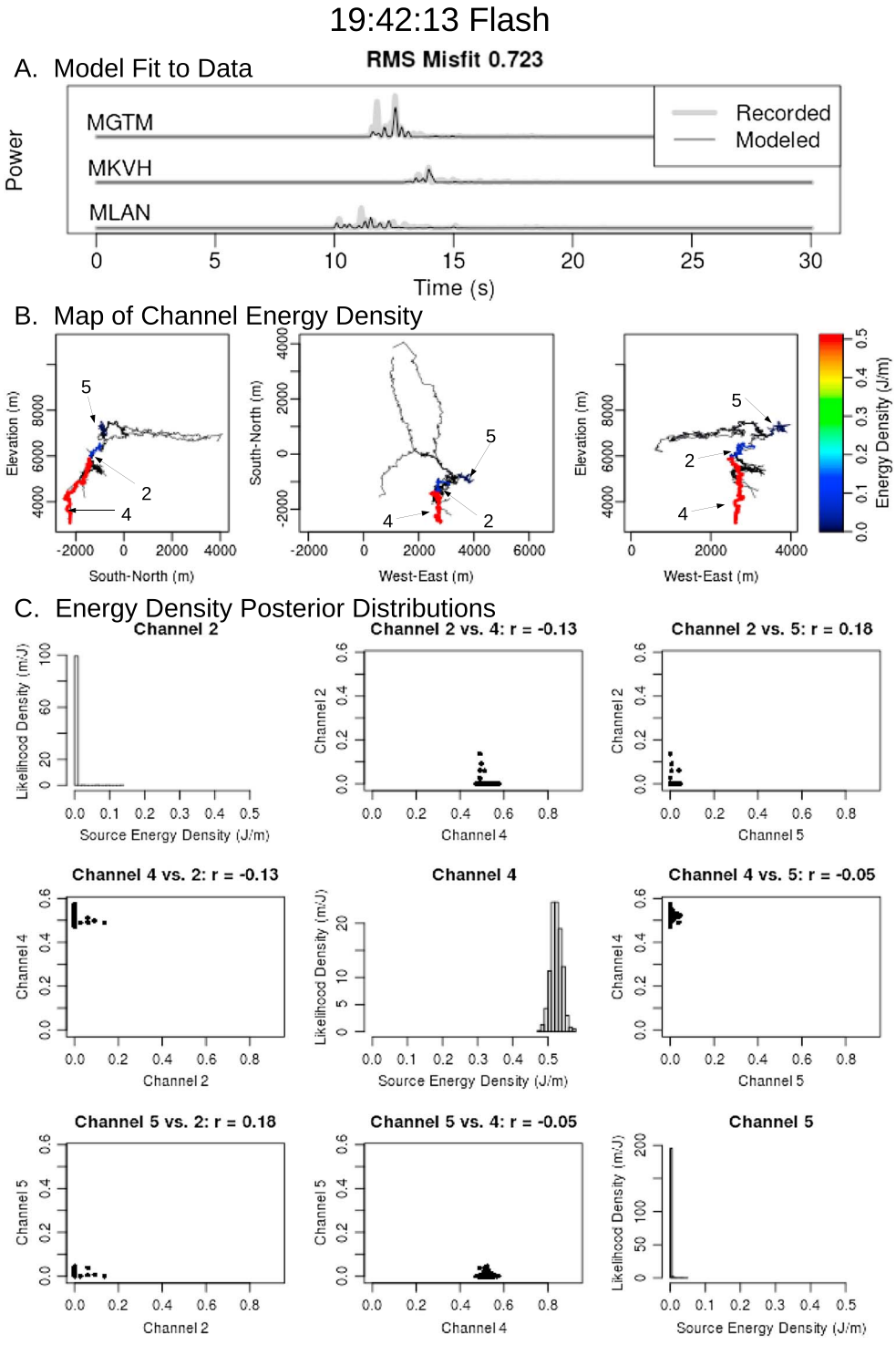

Figure 4. (a) Overlay of modeled and recorded thunder power envelopes for the CG flash at 19:42:13. (b) Map of inverted channel energy densities. (c) Posterior distributions of channel energy densities of thunder-producing channels. Channel 4, which is the direct channel to ground, produces the most thunder. Channels 2 and 5, which connect channel 4 to higher parts of the strike, produce little thunder.

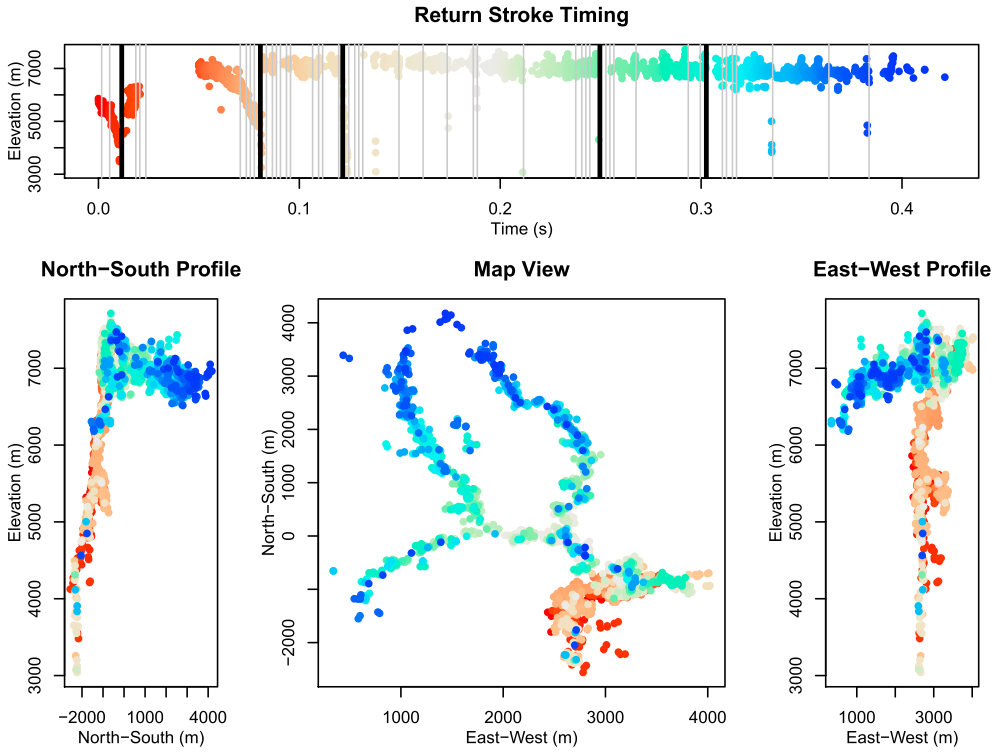

Figure 5. The evolution of the CG flash at 19:42:13 with time. Color of plotted points corresponds to VHF pulse times. Black vertical lines indicate times of major low-frequency radio pulses from return strokes; gray lines indicate smaller radio pulses. Most of the upper channels formed after the return strokes, making them unlikely to produce significant thunder.

this reduced the number of potential current-carrying channels to seven. These seven include one that extends all the way to ground, one that extends downward but fails to reach ground, two that propagate from above to meet the top of the ground strike, and three that extend horizontally away from the ground strike at high elevation (Figure 2).

Low-frequency radio interference from five significant current pulses (as well as many more smaller current pulses) was detected during this flash (Figure 5). However, the time intervals separating these pulses (0.05–0.2 s) are short compared to the duration of thunder signals and to the likely timing errors associated with propagation through complex atmospheres. Therefore, we find the average time of all strokes and use it as the sole source time in these calculations.

For each flash, we performed a grid search over many windless atmospheres with constant vertical sound speed gradients to find an optimal fit. Sound speed gradient varied from −0.006 to −0.0036 s^{-1}, and ground-level (3000 m above sea level) sound speed varied from 336 to 354 m s^{-1}. These correspond to temperature gradients of roughly 6–10°C km^{-1} and ground-level temperatures of roughly 9–41°C. Each atmosphere was tested using the inversion method described in the previous section. After identifying the atmosphere with the best fit, we performed a more detailed inversion on that atmosphere using 200,000 iterations instead of 50,000 and a burn-in period of 100,000 instead of 25,000. This was done in order to better characterize the posterior distributions of the source models.

Additionally, we tested five frequency bands for the flash that occurred at 19:42:13. The low corner of these bands ranged from 3 to 12 Hz, and the high corner was set to twice the low corner. We found that using the band from 6 to 12 Hz resulted in the lowest misfit for this flash. Additionally, synthetic data presented in the next section show that this band is the least susceptible to wind-related errors. Therefore, we picked this frequency band for analyzing other flashes.

We test many atmospheres to find an optimal fit between modeled and observed thunder, and it is worth noting that the atmosphere with the best fit is not necessarily the most correct atmosphere but rather the

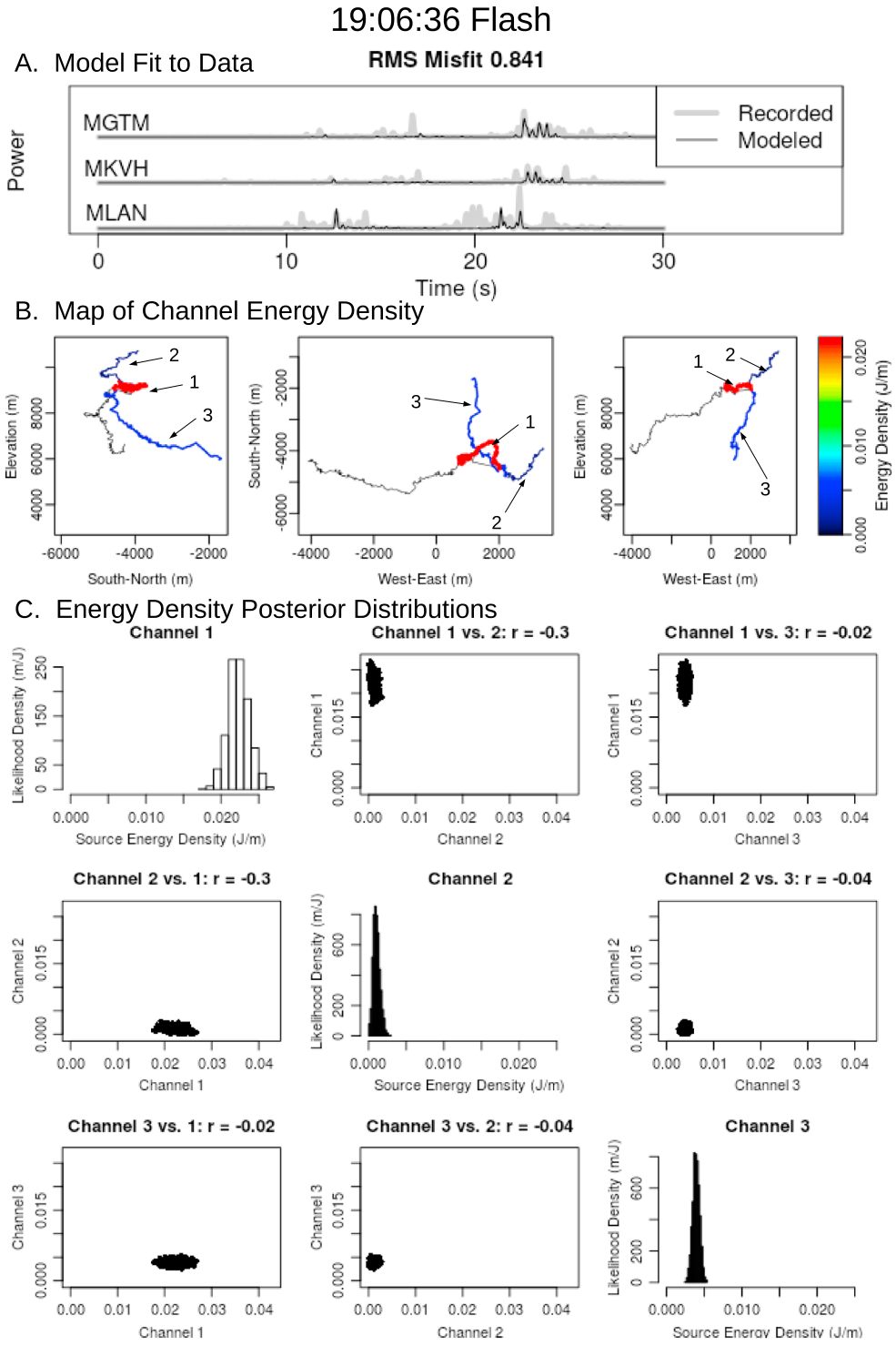

Figure 6. (a) Overlay of modeled and recorded thunder power envelopes for the IC flash at 19:06:36. (b) Map of inverted channel energy densities for the flash. (c) Posterior distributions of channel energy densities of thunder-producing channels. Channels 1 and 2 are somewhat correlated; this is a potential source of ambiguity in the results.

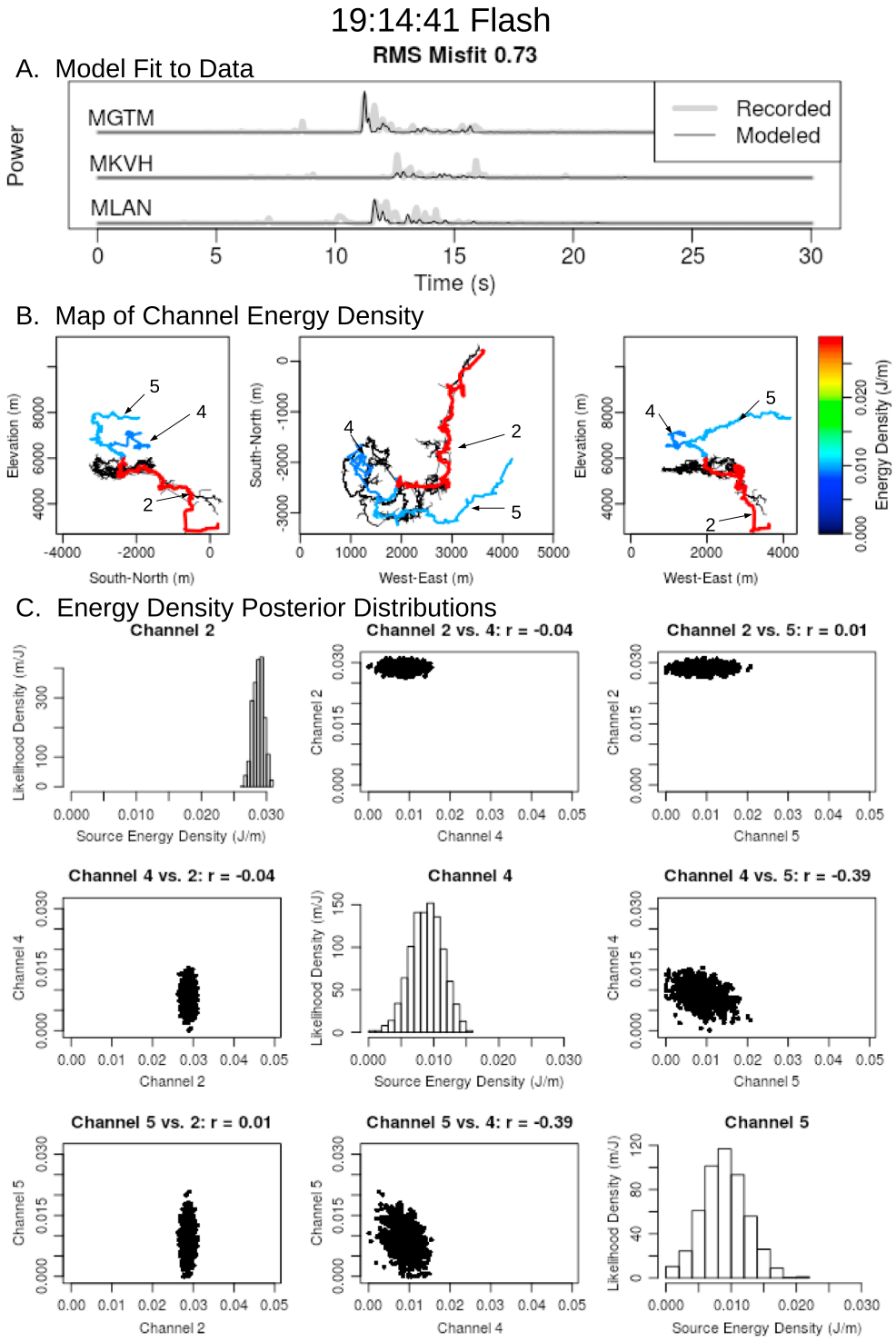

Figure 7. (a) Overlay of modeled and recorded thunder power envelopes for the 19:14:41 CG flash. (b) Map of inverted channel energy densities. The ground strike has the highest energy density; however, thunder is also detected from two upper channels. (c) Posterior distributions of channel energy densities. Energy densities of two upper channels are correlated, making distinguishing thunder from them difficult.

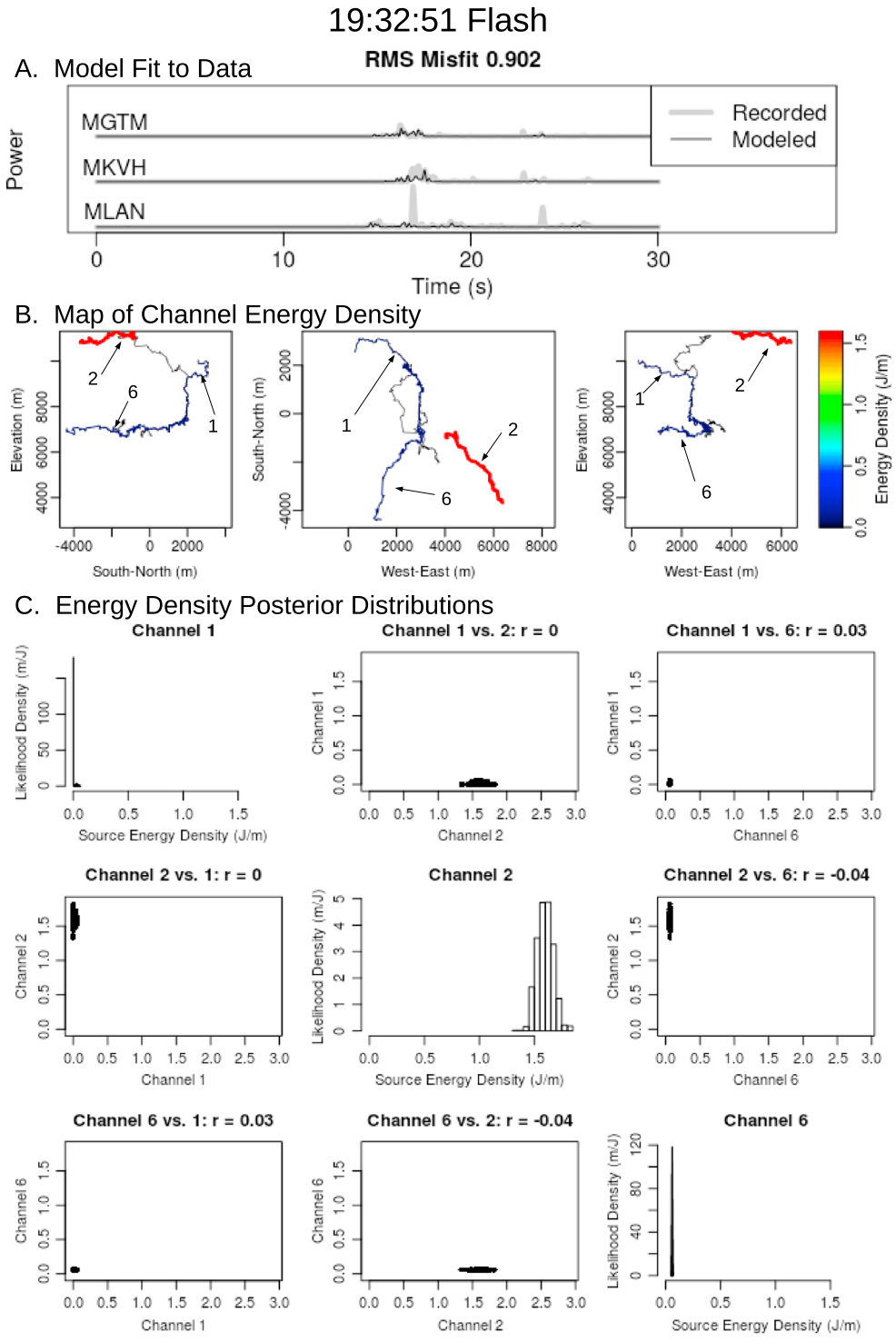

Figure 8. (a) Overlay of modeled and recorded thunder power envelopes for the 19:32:51 IC flash. (b) Map of inverted channel energy densities. Most energy is released by a high-elevation channel, but small amounts are also produced by other channels. (c) Posterior distributions of channel energy densities of thunder-producing channels.

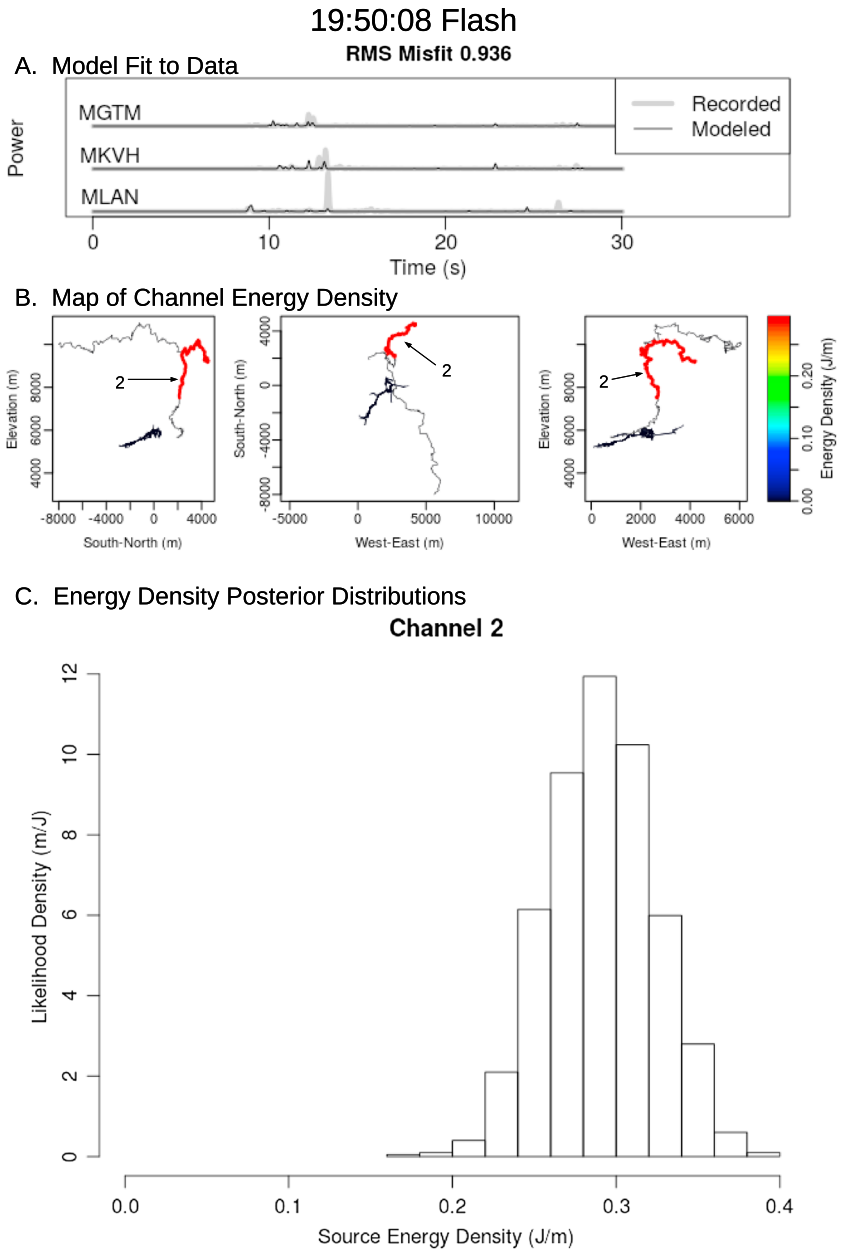

Figure 9. (a) Overlay of modeled and recorded thunder power envelopes for the 19:50:08 IC flash. (b) Map of inverted channel energy densities. (c) Posterior distribution of channel energy density of the thunder-producing channel (only one channel was found to produce any thunder in this flash).

very simplified atmosphere whose acoustic propagation effects best matched those of the very complicated true atmosphere. We describe best fit atmospheres of each flash in Table 1 but are reluctant to infer properties of the true atmosphere from them.

3.2. Results

We show results for six flashes (Figures 4–10). For each flash, the fit of modeled and recorded power envelopes is shown, along with the maximum-likelihood source amplitudes of the conductive channels constituting the flash and their posterior distributions.

The posterior distributions of the model parameters (diagonal subplots of Figures 4c, 6c, 7c, 8c, 9c, and 10c) are obtained from the detailed inversion; these show the likelihood distributions of the acoustic source amplitudes of different conductive channels and the covariance among them. A narrow distribution means

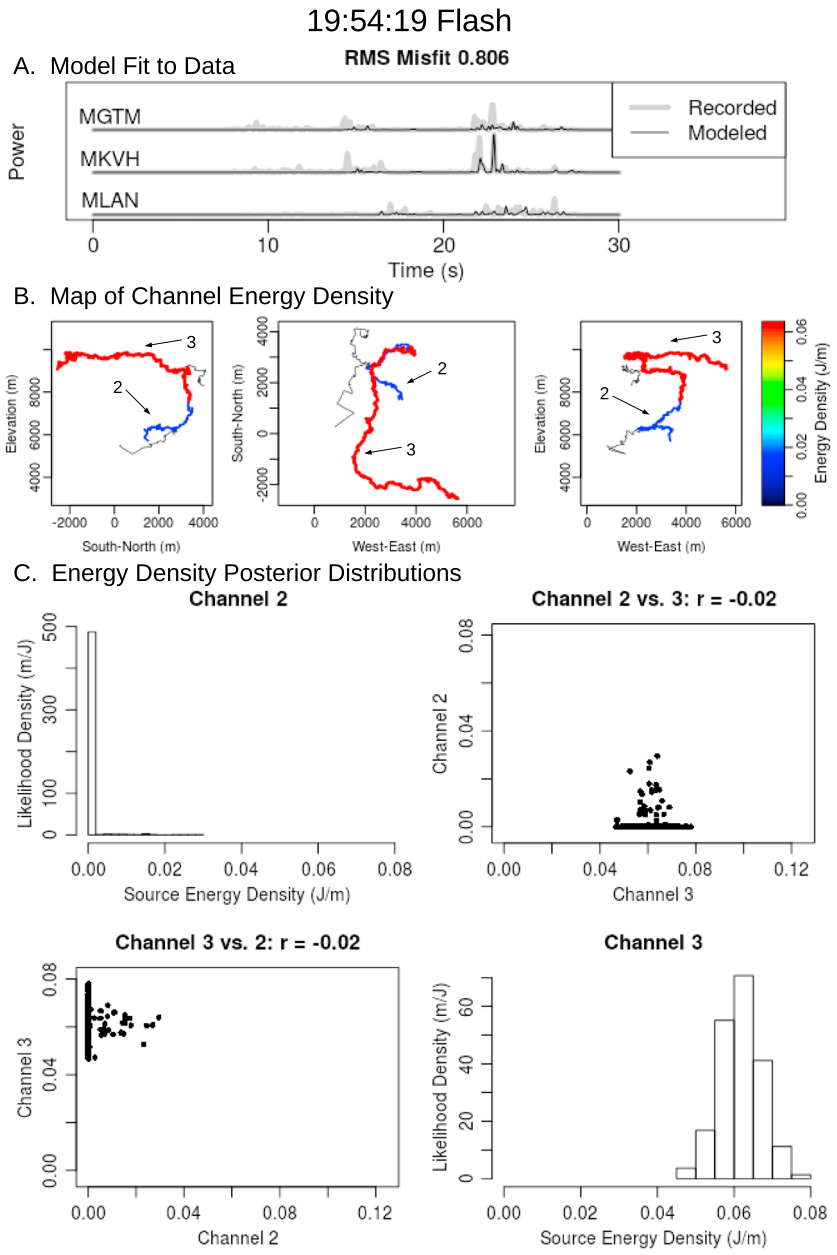

Figure 10. (a) Overlay of modeled and recorded thunder power envelopes for the 19:54:19 IC flash. (b) Map of inverted channel energy densities. (c) Posterior distributions of channel energy densities of thunder-producing channels. An upper channel 3 produces most thunder; contributions from the lower channel 2 are smaller and poorly resolved.

that the source amplitude has been resolved with high precision; a wide distribution means that the source amplitude could not be resolved very precisely. The off-diagonal subplots in those figures show relationships between inverted source amplitudes of different conductive channels; when a strong correlation exists, the source amplitudes of the two channels can trade off in a way that is difficult for the inversion to resolve.

3.3. Flash at 19:42:13

Detected thunder in this flash came from three mainly vertical channels extending toward ground (Figure 4). One of these is the original channel that extends from the initial breakdown to the ground; this produced the most thunder. Additionally, two subsequent channels formed from later breakdowns and connected to the top of the main ground strike; these produced much less thunder.

Interestingly, no thunder was detected from the long upper channels that propagated mainly horizontally. Considering the time of channel formation with respect to current pulse times (detected by low-frequency RF interference) can explain this finding (Figure 5). Glitches caused by RF interference synchronous with dart leaders are seen throughout the flash. More than half of these occur before the upper channels begin to form, and nearly all occur before the upper channels are fully formed. This indicates that these channels might not be major thunder sources because during most of the thunder-producing return strokes, the channels did not yet exist. On the other hand, the three channels that were found to produce thunder formed early in the strike.

3.4. Flash at 19:06:36

This IC flash includes two downward propagating channels, one channel that extends horizontally away from the initial breakdown and one that extends upward (Figure 6). All of these except one of the lower channels were found to produce thunder, and the midlevel, horizontal channel was the most energetic. Recovered energy densities of the lower and upper channels have a moderate negative correlation of −0.3, meaning that fit to recorded thunder may be roughly preserved by increasing energy density of one and decreasing it for the other. As a result, it is difficult to determine exactly how acoustic energy is partitioned between those two channels.

3.5. Flash at 19:14:41

This CG flash consists of a channel going to ground, along with a few horizontally propagating upper channels (Figure 7). Thunder from this flash is fit relatively well by models (normalized RMS misfit of 0.73). The ground strike is the most energetic channel, but two upper channels also produce substantial thunder. However, the recovered energy densities of the two upper channels are correlated ($r = -0.39$), meaning that energy density can be allocated to either and have a relatively small effect on model misfit.

3.6. Flash at 19:32:51

This IC flash consists of one main low-level channel, two upper level channels, and a single connection between the layers (Figure 8). One of the upper channels is calculated to produce the most thunder. A second upper channel and the low channel also produce measurable thunder. Fit of models to observations is relatively poor (RMS misfit of 0.9), meaning that much of the thunder cannot be explained by this method.

3.7. Flash at 19:50:08

This IC flash includes two high-elevation channels and two lower channels (Figure 9). Of these, only one channel (an upper channel) is found to produce any thunder. However, the misfit is high (0.936), meaning that some thunder-producing channels are not being identified because of unmodeled effects on waves they produce.

3.8. Flash at 19:54:19

This IC flash also consists of two upper channels and two lower channels (Figure 10). Thunder is detected prominently from one of the upper channels and ambiguously from a lower channel. The fit between modeled and recorded thunder is moderate (0.806).

4. Sensitivity of Method to Sources of Error

Monte Carlo simulations were performed in order to assess the importance of potential sources of error. The main sources of error are location uncertainty of RF pulses located by the LMA (addressed in section 4.1) and the unknown structure of the atmosphere (section 4.2). In each simulation, synthetic thunder was modeled for a realistic lightning strike (using the geometry of the 19:42:13 flash) and atmosphere. We then attempted to invert this signal for channel amplitude after adjusting the strike or atmosphere to reflect the source of error. We tested 12 frequency bands and source-of-error intensities, performed 20 trials for each combination, and calculated expected values for normalized data misfit (equation (1)) and normalized source model error

$$\frac{\|\mathbf{m}_{\text{True}} - \mathbf{m}_{\text{Inv}}\|_2}{N \cdot \|\mathbf{m}_{\text{True}}\|_2}, \tag{2}$$

where $\mathbf{m}_{\text{True}}$ is the true source model, $\mathbf{m}_{\text{Inv}}$ is an inverted source model, and N is the number of model parameters.

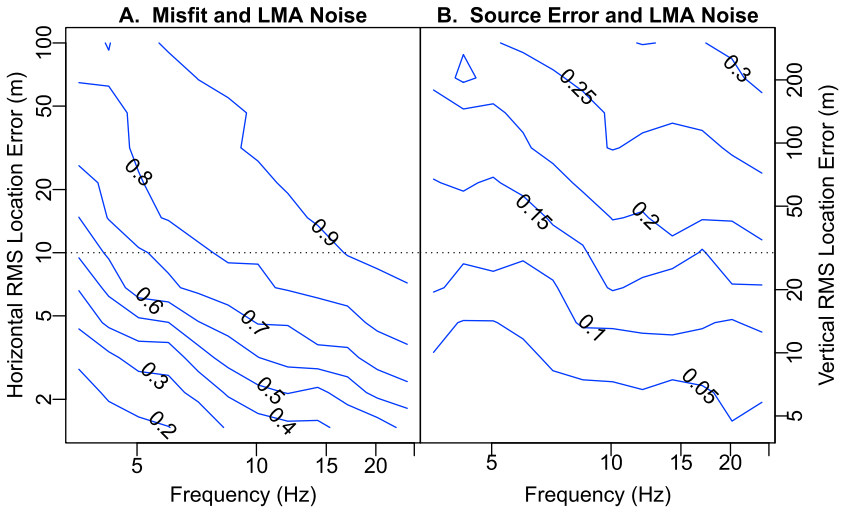

Figure 11. Contours showing the effect of LMA RF pulse location noise on inversions of synthetic data. Monte Carlo simulations revealed effects on (a) normalized misfit between prenoise and postnoise synthetic thunder and (b) errors between true and inverted amplitude (expressed as RMS residual between true and inverted amplitudes). Normalized thunder misfits increase with both the RMS location error and the corner frequency. However, errors in inverted channel amplitudes depend more strongly on RMS location error than on corner frequency. The true noise level for this LMA configuration is shown by the dashed horizontal line.

4.1. Sensitivity to RF Pulse Location Noise

RF pulse locations provided by the LMA inevitably contain some noise. In this configuration, horizontal and vertical location errors have standard deviations of 10 m and 30 m, respectively [*Thomas et al.*, 2004]. These errors affect travel times of modeled acoustic waves and alter thunder signals accordingly. Here we quantify the effect of RF pulse location noise on thunder signal recovery.

Twenty independent iterations were run for each frequency band and location noise level. In each iteration, thunder was forward modeled for the original RF pulse locations using the main downward reaching channel as the sole source. Then, RF pulses were offset by random errors distributed according to the standard deviations being tested. Finally, the modeled thunder and offset RF pulse locations were inverted using the frequency band being tested. We tested 12 location standard deviations and 12 frequency bands. Horizontal standard deviations ranged from 1.5 m to 100 m, with vertical standard deviation set to 3 times the horizontal standard deviation in each case. Central frequencies of the frequency bands ranged from 3.5 Hz to 24 Hz; in each case, the band's high corner was twice the low corner.

Figure 11 shows the dependence of misfit on frequency band and location standard deviation. The normalized misfit (equation (1)) was calculated for each simulation, and mean normalized misfits were calculated for each frequency standard deviation pair.

Additionally, we examine the effect of RF pulse location noise on accuracy of inverted channel amplitudes. Normalized error (equation (2)) between true and inverted channel amplitudes is strongly dependent on RF pulse location noise, and, to a lesser extent, corner frequency. These errors are generally between 0.1 and 0.2 for near-infrasound corner frequencies and realistic RF pulse location noise values. Notably, a high normalized misfit can correspond to a fairly low-error result; for example, in some cases, the normalized misfit was around 0.7 while the normalized error was around 0.1.

4.2. Sensitivity to Atmospheric Simplification

Thunderstorm atmospheric structure is complex, dynamic, and typically unknown. It is obviously impossible to test every possible atmospheric structure; with computation time being the main constraint, it is practical to only test windless atmospheres with constant sound speed gradients limited to the range in which thunderstorms typically develop. As a result, the difference between the tested atmosphere and true atmosphere is an important source of error.

We use a similar procedure to the previous test. The wind structure of the atmosphere from which thunder is generated is allowed to vary (with 12 different windiness levels), with a realistic and fixed sound speed

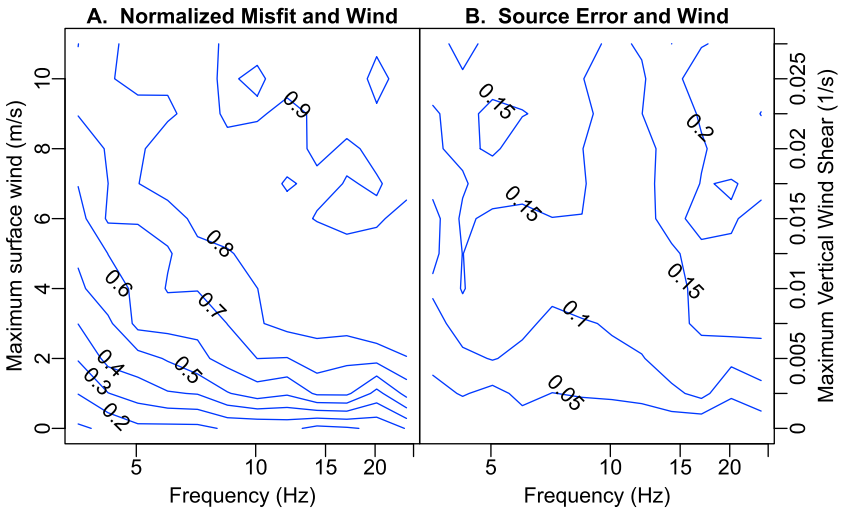

Figure 12. Effect of atmospheric wind intensity on (a) normalized misfit between true synthetic and inverted synthetic thunder and (b) accuracy of inverted channel amplitudes. Thunder misfit increases with corner frequency and maximum surface wind. However, true channel amplitudes can still be recovered reasonably accurately.

structure (surface sound speed of 343 m s^{-1} and vertical sound speed gradient of −0.005 s^{-1}). The windiest scenario tested has a surface wind of 11 m s^{-1} and a shear of 0.0275 s^{-1}. Winds during thunderstorms are highly variable, and we did not measure wind speeds or shear during the storm, but we consider this range to be illustrative of typical wind-related errors. For each windiness level, 12 frequency bands were tested with 20 iterations each. In each simulation, surface wind in a random direction was set to a random speed, with random wind shears chosen from an interval that depended on the windiness level being tested.

Thunder misfit increases rapidly with windiness and, to a lesser extent, corner frequency (Figure 12). However, these high misfits do not imply high normalized errors; over the range of atmospheres tested, expected error barely exceeds 0.25.

5. Discussion

Misfit between modeled and observed thunder varied among flashes (Table 1). We calculated normalized RMS misfits as low as 0.723 and as high as 0.936. So for some flashes, thunder could be reproduced fairly well, while for other flashes, little of the thunder could be modeled. Notably, CG flash thunder was reproduced much more reliably than IC thunder: misfits for both CG flashes were lower than misfits of any IC flashes. This could be related to the acoustic sources in IC flashes being higher (and therefore, more susceptible to atmospheric propagation effects) than those in CG flashes.

Table 1. Summary of Lightning Flashes Studied[a]

Time (UTC)	Type	Thunder-Producing Channels	Normalized Misfit	Energy Density (Jm^{-1})	Total Energy (J)	Basal Temperature (°C)	Temperature Gradient (°C m^{-1})
19:06:36	IC	3	0.841	2.22×10^{-2}	223	37.0	-9.1×10^{-3}
19:14:41	CG	3	0.73	2.89×10^{-2}	550	20.1	-1.0×10^{-2}
19:32:51	IC	3	0.902	1.60	12595	31.3	-9.1×10^{-3}
19:42:13	CG	3	0.723	5.12×10^{-1}	3379	22.2	-1.0×10^{-2}
19:50:08	IC	1	0.936	2.94×10^{-1}	3133	26.1	-9.0×10^{-3}
19:54:19	IC	2	0.806	6.35×10^{-2}	1761	30.9	-1.0×10^{-2}

[a]Data are from a 24 July 2009 thunderstorm. RMS misfit, energy density, total energy, best fit ground-level temperature, and best fit temperature gradient refer to values obtained by analyzing the 6–12 Hz frequency band. Basal temperature and temperature gradient correspond to the simplified windless test atmosphere for which the best model data fit was found; these values should not be interpreted as properties of the true atmosphere at the time of the flash.

The geometry of inverted acoustic sources in CG flashes is reasonable. In each CG flash studied, the channel from the initial breakdown toward ground was the most energetic acoustic source, while some higher channels produced thunder as well. While upper channels do not necessarily carry current, the channel to ground necessarily carries current in at least one return stroke in every strike, so this finding is unsurprising. In the flash at 19:42:13, the ground channel's energy density is much greater than the sum of the upper channels' energy densities. This indicates that most current flowed through the ground channel and that the return strokes carried by the upper channels were much less energetic. The CG flash at 19:14:41, on the other hand, has upper channels whose energy density sum is only slightly less than the energy density of the ground channel. This indicates that the upper channels were active during the most energetic return strokes, and most current flowed through both an upper and lower channel.

Because IC flashes do not involve a large conductive charge reservoir, their current pulses are less predictable. Consequently, it is difficult to assess whether a thunder source geometry for an IC event is reasonable. In the flash at 19:50:08, only a single channel was found to produce any thunder at all. However, in the 19:06:36 flash, three of the four channels produced substantial thunder.

Normalized misfits between recorded and modeled thunder are somewhat high in these flashes: no flash has a normalized misfit less than 0.73, and no IC flash has a normalized misfit less than 0.8. However, in the previous section, we determined that sources of error like VHF pulse location uncertainty and atmospheric winds could cause substantial thunder misfit while still allowing reasonably accurate estimates of source energy density. For example, assuming that wind is the main source of error, a ground-level wind of 3 m s^{-1} and a shear of 7.5×10^{-3} s^{-1} could cause a normalized thunder misfit of 0.7 but a normalized source amplitude error of only 0.1 (Figure 12). High thunder misfits do not necessarily indicate similarly inaccurate source energy estimates.

Other sources of error, such as echoes from topography and atmospheric heterogeneities more complicated than one-dimensional linear variations with elevation could potentially reduce the accuracy of this method. For example, a ground-level inversion could preferentially focus waves from low-elevation sources to receivers. Wave propagation models would not predict this and would therefore overestimate energy density of low channels while underestimating high channels. Such structures are common near downdrafts in storms, so this may be a common source of error for this technique. Similarly, a local vertical wind or turbulent region might distort thunder signals from nearby channels, causing those channels' source energies to be underestimated by the inversion. Topographic echoes might have the opposite effect: the coincident arrival of direct waves from one channel and a topographic echo from a different channel could not be predicted without a more complex propagation model; lacking one, all arriving energy would be attributed to the direct waves, and the energy of the channel producing them would be overestimated.

The source energy densities found in this work (between 2×10^{-2} Jm^{-1} and 1.6 Jm^{-1}) may seem low for lightning strikes carrying current on the order of 3×10^4 A (Table 1). However, several factors must be considered, first being that the channels are very long (thousands of meters) and energy is radiated along their entire length, so the total energy released is, in these units, 3–4 orders of magnitude higher than the energy density. Further, we are looking only at a narrow frequency band (6–12 Hz) that carries only a small fraction of the total thunder energy. Finally, thunder generation is highly inefficient: most input energy is dissipated in shock wave decay close to the channel. So these seemingly low thunder energy densities do not conflict with the enormous amount of energy involved in lightning.

6. Conclusion

We have introduced a new method for locating thunder sources and current flow within a lightning flash by joint inversion of synchronous thunder recordings and RF pulse catalogs from the LMA. This method involves connecting RF pulses to reconstruct conductive channels created by leaders, modeling acoustic signals produced by each conductive channel, and inverting using a Monte Carlo Markov Chain to determine the source energy density of each conductive channel in order to minimize misfit between modeled and recorded thunder power envelopes. The returned posterior distribution of channel energy density can be used to distinguish thunder-producing channels from silent channels.

Sources of error in this method include LMA RF pulse location noise and complications in atmospheres. Typical levels of LMA RF pulse location noise have little effect on accuracy of recovered channel energy densities.

The effect of high winds is more significant. Additionally, effects of turbulence and topography could cause errors that are difficult to quantify, while intrinsic attenuation could potentially cause errors for frequencies higher than those studied here.

We applied this method to lightning flashes that occurred on 24 July 2009 in the Magdalena Mountains, New Mexico, USA. Thunder from CG flashes was reproduced more reliably than thunder from IC flashes. The misfit observed in some flashes is similar to expected values for moderately windy atmospheres, for which source energy estimate errors are expected to be close to 25%. In most strikes, multiple channels produced thunder, and in all strikes, at least one channel produced no thunder.

Current flow in lightning is a powerful and often destructive process, and this project enables its study by combining RF and acoustic observations. The method's sensitivity to atmospheric structure means that accuracy could be improved by incorporating meteorological data. Radiosondes, meteorological models, or other constraints on atmospheric structure near flashes will improve the accuracy of this method. Additionally, knowing the true atmospheric structure would eliminate the need to test many atmospheres; however, as the true atmosphere in and around the storm will contain three-dimensional structure, the need to use a more complex and computationally expensive three-dimensional propagation model would increase runtimes and memory needs of this method along with its accuracy. Future work might include current measurements and shock wave modeling to study energy conversion along conductive channels or determining characteristics of channels that tend to carry current.

Acknowledgments

E. Badillo, R. Johnson, J. Michnovicz, and M. Murray participated in fieldwork and H. Edens provided RF pulse locations from the LMA. This work was funded by NSF grant AGS-0934472. Thunder and LMA data are available upon request to the authors.

References

Anderson, J. (2013), AtmRay: Acoustic traveltime calculations for 1-D atmospheric models, *R package version 1.31*, http://cran.rproject.org/web/packages/AtmRay/index.html.

Arechiga, R. O., J. B. Johnson, H. E. Edens, R. J. Thomas, and W. Rison (2011), Acoustic localization of triggered lightning, *J. Geophys. Res.*, *116*, D09103, doi:10.1029/2010JD015248.

Aster, R. C., B. Borchers, and C. H. Thurber (2012), *Parameter Estimation and Inverse Problems*, Elsevier Acad. Press, Waltham, Mass.

Balachandran, N. K. (1979), Infrasonic signals from thunder, *J. Geophys. Res.*, *84*, 1735–1745.

Balachandran, N. K. (1983), Acoustic and electric signals from lightning, *J. Geophys. Res.*, *88*, 3879–3884.

Bohannon, J. L., A. A. Few, and A. J. Dessler (1977), Detection of infrasonic pulses from thunderclouds, *Geophys. Res. Lett.*, *4*, 49–52.

de Groot-Hedlin, C. (2008), Finite-difference time-domain synthesis of infrasound propagation through an absorbing atmosphere, *J. Acoust. Soc. Am.*, *124*, 1430–1441.

Dessler, A. J. (1973), Infrasonic thunder, *J. Geophys. Res.*, *78*, 1889–1896.

Few, A. A. (1969), Power spectrum of thunder, *J. Geophys. Res.*, *74*, 6926–2934.

Few, A. A. (1970), Lightning channel reconstruction from thunder measurements, *J. Geophys. Res.*, *75*, 7517–7523.

Few, A. A. (1974), Thunder signatures, *EOS Trans. AGU*, *55*, 508–514.

Few, A. A., and T. L. Teer (1974), The accuracy of acoustic reconstruction of lightning channels, *J. Geophys. Res.*, *79*, 5007–5011.

Fleagle, R. G (1949), The audibility of thunder, *J. Acoust. Soc. Am.*, *21*, 411–412.

Garces, M. A., R. A. Hansen, and K. G. Lindquist (1998), Traveltimes for infrasonic waves propagating in a stratified atmosphere, *Geophys. J. Int.*, *135*, 255–263.

Hastings, W. K. (1970), Monte Carlo sampling methods using Markov chains and their applications, *Biometrika*, *57*, 97–109.

Holmes, C. R., M. Brook, P. Krehbiel, and R. McCrory (1971), On the power spectrum and mechanism of thunder, *J. Geophys. Res.*, *76*, 2106–2115.

Johnson, J. B., R. O. Arechiga, R. J. Thomas, H. E. Edens, J. F. Anderson, and R. L. Johnson (2011), Imaging thunder, *Geophys. Res. Lett.*, *38*, L19807, doi:10.1029/2011GL049162.

Johnson, R. L. (2012), Characteristics of thunder and relationships to lightning sources in the Magdalena Mountains, central New Mexico, Master's thesis, New Mexico Inst. of Mining and Tech., Socorro, N. M.

MacGorman, D. R., A. A. Few, and T. L. Teer (1981), Layered lightning activity, *J. Geophys. Res.*, *86*, 9900–9910.

Marcillo, O., J. B. Johnson, and D. Hart (2012), Implementation, characterization, and evaluation of an inexpensive low-power low-noise infrasound sensor based on a micromachined differential pressure transducer and a mechanical filter, *J. Atmos. Oceanic Technol.*, *29*, 1275–1284.

Otterman, J. (1959), Finite-amplitude propagation effect on shock-wave travel times from explosions at high altitudes, *J. Acoust. Soc. Am.*, *31*, 470–474.

Rakov, V. A., and M. A. Uman (2003), *Lightning: Physics and Effects*, Cambridge Univ. Press, Cambridge, U. K.

Rison, W., R. J. Thomas, P. R. Krehbiel, T. Hamlin, and J. Harlin (1999), A GPS-based three-dimensional lightning mapping system: Initial observations in central New Mexico, *Geophys. Res. Lett.*, *26*, 3573–3576.

Sutherland, L. C., and H. E. Bass (2004), Atmospheric absorption in the atmosphere up to 160 km, *J. Acoust. Soc. Am.*, *115*, 1012–1032.

Teer, T. L., and A. A. Few (1974), Horizontal lightning, *J. Geophys. Res.*, *79*, 3436–3441.

Thomas, R. J., P. R. Krehbiel, W. Rison, S. J. Hunyady, W. P. Winn, T. Hamlin, and J. Harlin (2004), Accuracy of the Lightning Mapping Array, *J. Geophys. Res.*, *109*, D14207, doi:10.1029/2004JD004549.

Uman, M. A. (1987), *The Lightning Discharge*, Acad. Press, Orlando, Fla.

Valine, W. C., and E. P. Krider (2002), Statistics and characteristics of cloud-to-ground lightning with multiple ground contacts, *J. Geophys. Res.*, *107*, 4441, doi:10.1029/2001JD001360.